J. Fluid Mech. (1989), *vol.* 199, *pp.* 133–154
Printed in Great Britain

The effects of boundary imperfections on convection in a saturated porous layer: near-resonant wavelength excitation

By D. A. S. REES† AND D. S. RILEY‡

†Department of Mathematics, North Park Road, Exeter EX4 4QE, UK

‡School of Mathematics, University Walk, Bristol BS8 1TW, UK

Weakly nonlinear theory is used to study the porous-medium analogue of the classical Rayleigh–Bénard problem, i.e. Lapwood convection in a saturated porous layer heated from below. Two particular aspects of the problem are focused upon: (i) the effect of thermal imperfections on the stability characteristics of steady rolls near onset; and (ii) the evolution of unstable rolls.

For Rayleigh–Bénard convection it is well known (see Busse and co-workers 1974, 1979, 1986) that the stability of steady two-dimensional rolls near onset is limited by the presence of cross-roll, zigzag and sideband disturbances; this is shown to be true also in Lapwood convection. We further determine the modifications to the stability boundaries when small-amplitude imperfections in the boundary temperatures are present. In practice imperfections would usually consist of broadband thermal noise, but it is the Fourier component with wavenumber close to the critical wavenumber for the perfect problem (i.e. in the absence of imperfections) which, when present, has the greatest effect due to resonant forcing. This particular case is the sole concern of the present paper; other resonances are considered in a complementary study (Rees & Riley 1989).

For the case when the modulations on the upper and lower boundaries are in phase, asymptotic analysis and a spectral method are used to determine the stability of roll solutions and to calculate the evolution of the unstable flows. It is shown that steady rolls with spatially deformed axes or spatially varying wavenumbers evolve. The evolution of the flow that is unstable to sideband disturbances is also calculated when the modulations are π out of phase. Again rolls with a spatially varying wavenumber result.

1. Introduction

The study of the effects of small imperfections on classical flows such as Bénard convection has received much attention in the last decade or so (see, for example, Kelly & Pal 1976, 1978; Pal & Kelly 1978, 1979; Vozovoi & Nepomnyaschii 1974; Walton 1982; Eagles 1980; Rees & Riley 1986; Hall & Walton 1977, 1979; Daniels 1982; and Zaleski 1984). These analyses have, in part, been motivated by a desire to model experimental imperfections such as thermal noise, and boundary misalignment or roughness. Additionally, the results have been of considerable interest in the context of bifurcation theory and the study of nonlinear systems in general. In this context we may view the present study as one of determining the unfolding of the bifurcation structure arising in a problem possessing $\mathbb{Z}_2$ reflectional symmetry (up–down symmetry) and a continuous transformation group (arbitrary shifts in the horizontal direction).

Recently, in a series of experiments, Lowe, Gollub and co-workers (Lowe, Gollub & Lubensky 1983; Lowe & Gollub 1985*a*, *b*; Lowe, Albert & Gollub 1986) have found a number of novel cellular patterns in thin layers of nematic liquid crystal subjected to a spatially periodic potential difference. Their striking structures may be related to the effects of competing frequencies or periodicities, namely, those of the forcing and of the usual Bénard thermo-convective instability. It is important that we have a theoretical framework within which we can explain the complex spatial patterns resulting from the interplay between incommensurate lengthscales.

In this paper we report the findings of a study into the effects of boundary thermal noise on convection in an infinite porous layer heated from below and cooled from above. The results also apply qualitatively to the corresponding Boussinesq-fluid problem (Wynne 1987). Now, in practice, imperfections often consist of two-dimensional broadband thermal noise containing many different Fourier components. In this study, however, we assume, for simplicity, that the thermal noise at both boundaries is steady and varies periodically in one spatial direction only. Under these assumptions Rees & Riley (1989) find that the Fourier component with wavenumber k_w close to the critical wavenumber, k_c, of the perfect problem (i.e. when imperfections are absent) has the greatest effect when the Rayleigh number is near Ra_c, the critical value for the perfect problem. We focus on the effects of this particular component; when it is absent other resonances become important and this is taken up in a complementary study (Rees & Riley 1989). The k_w-mode modulation at the boundaries may be factored into in-phase and π-out-of-phase components, and the effect of the imperfections depends crucially on this factorization. If there is in-phase (or sinuous) thermal modulation at the boundaries then its effects dominate those caused by the other component and all other Fourier modes, at least to the order considered here. When the in-phase component is absent, the varicose, or π-out-of-phase, component must be considered in isolation as varicose components of other wavelengths can dominate. We shall concentrate upon the k_w-mode imperfection: the in-phase case is studied in §§3, 4 and 5, whilst the out-of-phase case is studied in §6.

At small non-zero values of the Rayleigh number, Ra, a unique two-dimensional cellular convection of wavenumber k_w and amplitude $O(\epsilon)$ exists, where ϵ is a measure of the small-amplitude thermal imperfection. In the sinuous case, as the Rayleigh number approaches Ra_c, there is a smooth transition to a finite-amplitude convective regime, which is also two-dimensional and has wavenumber k_w. Our aims are to derive conditions for the stability of this basic flow, and, when unstable, to find the ultimate steady solutions that evolve. These aims are most easily achieved by using the evolution equations which govern the amplitude of the flow. Rees & Riley (1989) show that to balance the effects of a detuned boundary forcing and the thermo-convective instability in the evolution equations the scalings $k_w - k_c = \epsilon^{\frac{1}{3}}K$ and $Ra - Ra_c = \epsilon^{\frac{2}{3}}R$ are needed. Three different instability mechanisms, namely, the cross-roll, zigzag and sideband instabilities (see Busse & Whitehead 1974; Busse & Clever 1979; Bolton, Busse & Clever 1986), are analysed separately in §§3, 4 and 5, respectively. In practice, all three mechanisms may be present and interact; we therefore consider this work to be a first step in understanding the evolution of these instabilities in the presence of non-uniformities.

When the basic roll is unstable to the cross-roll instability, the flow evolves monotonically to a new state. The original roll decays in amplitude and the disturbances grow to produce a mixed-mode convection pattern reminiscent of the bimodal convection pattern found by Busse & Whitehead (1971). It is found that,

owing to the presence of the imperfection, there is a continuous finite band of wavenumbers for which the basic roll is no longer unstable to the cross-roll disturbance. Thus Straus' stability envelope (Straus 1974) is modified near its lower vertex and the size of the stable region is increased. The bifurcation to the mixed mode may be either supercritical or subcritical; for certain values of k_w, therefore, it is possible to have hysteresis between the mixed mode and the original roll as Ra varies.

When the roll becomes unstable to the zigzag instability, a new flow arises at a supercritical bifurcation. It is found that stable rolls exist with wavenumber k_w less than k_c, in contrast to the perfect case. Thus again the imperfections serve to stabilize the basic roll. Unlike the evolution of the cross-roll instability which could be followed analytically, here we have to resort to numerical methods. By using a simple Galerkin scheme, the amplitude equation is transformed from a partial differential equation to an infinite set of coupled nonlinear ordinary differential equations in time. This is truncated and solved numerically using a standard library routine. It is found that there are two distinct steady solutions that can evolve: both have spatially deformed axes, but differ in their mean alignments. In general, when (Ra, k_w) lies close to the marginal curve the mean alignment is along the basic roll axis, but when (Ra, k_w) is far from the curve it is at an angle that is $O(\epsilon^{\frac{1}{2}})$ to this. Under certain conditions it is possible for both to be stable solutions, the one that is realized depends on the initial conditions, and once more, hysteresis is possible.

When the layer is sufficiently restricted in the spanwise direction neither of the above instabilities can be accommodated within the layer. In this case the only instability to which the basic roll can be subject is the sideband instability. This instability is also important when considering the associated problem of the stability of convection in a thermally modulated, shallow Hele-Shaw cell, since the flow is essentially two-dimensional and identical non-dimensional equations hold. Again, the stability boundary is modified from that for the perfect problem, and it is shown analytically that the bifurcations corresponding to points on the marginal stability curve may be either supercritical or subcritical depending on the precise position on the curve. The evolution of the sideband disturbances is followed using a similar method to that used for the zigzag instability. In this case we obtain a unique evolved state: a roll, the wavenumber of which varies in space.

When the thermal modulations at the boundaries are π out of phase then there is no longer a smooth transition to finite-amplitude convection near Ra_c, rather the weak subcritical flow loses its stability and bifurcates to finite-amplitude convective motion. Thus in this case the imperfection is 'weak': the bifurcation is not unfolded as the imperfection does not remove the symmetry broken at the bifurcation point. In general, the resultant motion is three-dimensional with the mode of lowest critical Rayleigh number ($O(\epsilon)$ *below* Ra_c) consisting of rectangular cells. If, however, the layer is sufficiently restricted in the spanwise direction, then this pattern cannot fit into the layer. We assume this restriction holds, or we notionally consider Hele-Shaw motions, and focus on two-dimensional flows.

The appropriate scalings for this case are $k_w - k_c = \epsilon K$ and $Ra - Ra_c = \epsilon^2 R$ (Rees & Riley 1989). We find that there are two different roll solutions that can evolve: one corresponds to a single roll with wavenumber k_w and occurs when K is small, the other is a flow with a spatially varying wavenumber and occurs for larger values of K. The latter flow arises either from the instability of the former or as a result of the evolution of a pair of small-amplitude disturbances with wavenumbers $k_w \pm \epsilon L$.

2. Formulation of the problem and derivation of the amplitude equations

We consider a horizontal porous layer of infinite extent saturated with a Boussinesq fluid and heated from below. The flow configuration and coordinate system are sketched in figure 1. On assuming that the Prandtl–Darcy number is large, and that the fluid and the matrix are in local thermal equilibrium, convective flows are governed by the non-dimensional equations (see Rees & Riley 1986):

$$\nabla\cdot\boldsymbol{q} = 0, \tag{2.1}$$

$$\theta_t + (\boldsymbol{q}\cdot\nabla)\theta = \nabla^2\theta, \tag{2.2}$$

$$\boldsymbol{q} = -\nabla p + Ra\,\theta\hat{\boldsymbol{z}}, \tag{2.3}$$

where $\hat{\boldsymbol{z}}$ is the upward unit normal, p the pressure, θ the temperature and $\boldsymbol{q}$ the Darcy velocity vector. Here the variables have been non-dimensionalized with respect to length, velocity, pressure, temperature and time scales given by d, $\lambda_m/(\rho_f c_f d)$, $\nu\lambda_m/(K^* c_f)$, ΔT, and $\rho_m c_m d^2/\lambda_m$, respectively, where λ_m, ρ_m, c_m are the effective thermal conductivity, density and specific heat of the saturated medium, and ν and c_f are the kinematic viscosity and specific heat of the saturating fluid, which has reference density ρ_f. The Rayleigh number is given by $Ra = \beta g K^* \Delta T d\rho_f c_f/\nu\lambda_m$, where β is the coefficient of cubical expansion of the saturating fluid, g the acceleration due to gravity, K^* the permeability, ΔT half the mean temperature drop across the layer, and d the half-width of the layer. The elimination of $\boldsymbol{q}$ from these equations yields

$$\nabla^2 p = Ra\,\theta_z, \tag{2.4}$$

$$\nabla^2\theta = Ra\,\theta\theta_z - \nabla p\cdot\nabla\theta + \theta_t. \tag{2.5}$$

We assume that the boundary temperatures have small-amplitude sinusoidal variations about their mean values. We consider variations that are either sinuous (antisymmetric) or varicose (symmetric) with common wavenumber k_w close to k_c. Thus the non-dimensional boundary conditions on $z = \pm 1$ are

$$\theta = \mp 1 + \tfrac{1}{2}\epsilon(e^{ik_w x} + e^{-ik_w x}) \quad \text{(sinuous)}, \tag{2.6}$$

$$\theta = \mp 1 \pm \tfrac{1}{2}\epsilon(e^{ik_w x} + e^{-ik_w x}) \quad \text{(varicose)}, \tag{2.7}$$

$$p_z = Ra\,\theta, \tag{2.8}$$

where $\epsilon \ll 1$. We further assume there is no net horizontal volumetric flux.

When the Rayleigh number is sufficiently below Ra_c the fluid motion is driven solely by the boundary thermal non-uniformities, and is therefore two-dimensional. This we term the quasi-conduction regime, full details of which are given in Rees & Riley (1989). In this paper we employ weakly nonlinear theory to study the effects of the boundary imperfections when Ra is close to Ra_c and $k_w \sim k_c$; Rees & Riley (1989) consider the complementary case $k_w \nsim k_c$.

In the sinuous case, the appropriate convective scale is $O(\epsilon^{\frac{1}{3}})$ (cf. Rees & Riley 1986, 1989; Tavantzis, Reiss & Matkowsky 1978; and Kelly & Pal 1978), and we expand the solutions to (2.4), (2.5) in powers of $\epsilon^{\frac{1}{3}}$:

$$(p, \theta, Ra) = \sum_{n=0} \epsilon^{n/3}(p_n, \theta_n, R_n), \tag{2.9}$$

where the conduction solution is

$$(p_0, \theta_0, R_0) = (-\tfrac{1}{2}Ra_c z^2, -z, Ra_c). \tag{2.10}$$

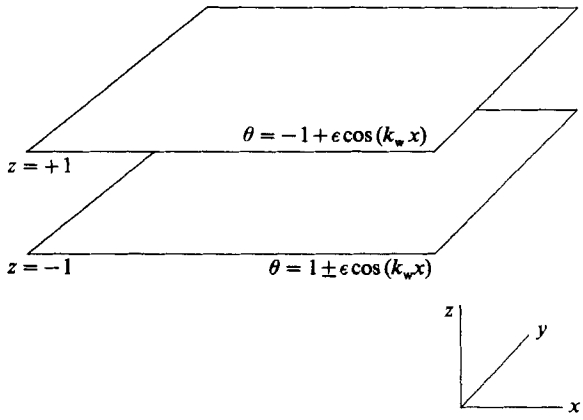

FIGURE 1. A sketch of the flow configuration and coordinate system.

For longitudinal rolls, the first-order eigensolution is taken to be

$$\begin{pmatrix} p_1 \\ \theta_1 \end{pmatrix} = \tfrac{1}{2}\mathrm{i}[A(X,Y,\tau)\,\mathrm{e}^{\mathrm{i}k_c x} - \bar{A}(X,Y,\tau)\,\mathrm{e}^{-\mathrm{i}k_c x}]\begin{pmatrix} 2k_c \sin(k_c z) \\ \cos(k_c z) \end{pmatrix}, \tag{2.11}$$

where $X = \epsilon^{\frac{1}{3}}x$, $Y = \epsilon^{\frac{1}{2}}y$, $\tau = \frac{1}{2}\epsilon^{\frac{2}{3}}t$, and the overbar denotes complex conjugation. After setting $k_w = k_c + \epsilon^{\frac{1}{3}}K$ in order to investigate the effects of small detunings of the boundary wavenumber from k_c, the solvability condition at $O(\epsilon)$ yields a Landau–Ginzburg equation governing the amplitude A:

$$A_\tau = RA + \left[2\frac{\partial}{\partial X} - \frac{\mathrm{i}}{k_c}\frac{\partial^2}{\partial Y^2}\right]^2 A - k_c^4 A^2\bar{A} - 4\mathrm{i}k_c\,\mathrm{e}^{\mathrm{i}KX}, \tag{2.12}$$

where $R = R_2$ and $R_1 = 0$. This equation may be made consistent with the notation of Rees & Riley (1986) by introducing the substitutions $A = -\mathrm{i}2^{\frac{1}{3}}A^*$, $X = 2^{-\frac{1}{3}}X^*$, $Y = 2^{-\frac{1}{6}}Y^*$, $R = 2^{\frac{2}{3}}R^*$, $K = 2^{\frac{1}{3}}K^*$, $\tau = 2^{-\frac{2}{3}}\tau^*$, which yield, on omitting the superscripts,

$$A_\tau = RA + \left[2\frac{\partial}{\partial X} - \frac{\mathrm{i}}{k_c}\frac{\partial^2}{\partial Y^2}\right]^2 A - k_c^4 A^2\bar{A} + 2k_c\,\mathrm{e}^{\mathrm{i}KX}. \tag{2.13}$$

In §3 the interaction of longitudinal and oblique rolls is considered. For this case the first-order eigensolution is taken to be

$$\begin{pmatrix} p_1 \\ \theta_1 \end{pmatrix} = \tfrac{1}{2}\mathrm{i}[(A(X,\tau)\,\mathrm{e}^{\mathrm{i}k_c x} - \text{c.c.}) + (B(X_b,\tau)\,\mathrm{e}^{\mathrm{i}k_c x_b} - \text{c.c.})]\begin{pmatrix} 2k_c \sin(k_c z) \\ \cos(k_c z) \end{pmatrix}, \tag{2.14}$$

where $x_b = x\cos\Phi - y\sin\Phi$, and $X_b = \epsilon^{\frac{1}{3}}x_b$. At $O(\epsilon)$ the application of solvability conditions yields a pair of amplitude equations for the amplitudes A and B:

$$A_\tau = RA + 4A_{XX} - k_c^4 A(|A|^2 + \Omega|B|^2) + 2k_c\,\mathrm{e}^{\mathrm{i}KX}, \tag{2.15a}$$

$$B_\tau = RB + 4B_{X_bX_b} - k_c^4 B(|A|^2 + \Omega|B|^2), \tag{2.15b}$$

where we have again omitted the subscripts. Here Ω is a function of Φ, the $O(1)$ angle between the roll axes, and is given by

$$\Omega(\Phi) = \frac{70 + 28\cos^2\Phi - 2\cos^4\Phi}{49 - 2\cos^2\Phi + \cos^4\Phi}. \tag{2.16}$$

$\Omega(\Phi)$ attains a maximum value of 2 at $\Phi = 0$ (parallel rolls) and a minimum value of 10/7 when $\phi = \frac{1}{2}\pi$ (perpendicular rolls).

In the varicose case, the appropriate roll-amplitude scale is $O(\epsilon)$ (Rees & Riley 1986, 1989), and we expand the solutions in powers of ϵ:

$$(p, \theta, Ra) = \sum_{n=0} \epsilon^n (p_n, \theta_n, R_n), \tag{2.17}$$

where the conduction solution is again given by (2.10). The first-order eigensolution is again taken to be (2.11) but now $X = \epsilon x$ and $\tau = \frac{1}{2}\epsilon^2 t$. In this case we consider only the two-dimensional stability of the longitudinal roll and consider A to be independent of Y. After setting $k_w = k_c + \epsilon K$, the solvability condition at $O(\epsilon^3)$ yields

$$A_\tau = (R - I_4) A + I_5 \bar{A} e^{2iKX} + 4A_{XX} - k_c^4 A^2 \bar{A}, \tag{2.18}$$

where $I_4 = -3.80429$ and $I_5 = 0.95773$.

3. The cross-roll instability for the sinuous configuration

From (2.13) the equation governing the amplitude of weakly nonlinear two-dimensional roll cells is given by

$$A_\tau = RA + 4A_{XX} - k_c^4 A^2 \bar{A} + 2k_c e^{iKX}. \tag{3.1}$$

It may be noted that the form of this equation is identical in structure to that proposed recently by Coullet (1987). The most trivial steady solution is given by the 'phase-winding' solution

$$A = A_0 e^{iKX}, \tag{3.2}$$

where A_0 is real and satisfies the equation

$$(R - 4K^2) A_0 - k_c^4 A_0^3 + 2k_c = 0. \tag{3.3}$$

When $R > 3k_c^2 + 4K^2$ there are three solution branches, of which the disconnected secondary branches are both unstable in a horizontally unbounded layer.

The stability of the roll defined by (3.2) to a disturbance in the form of a roll aligned at an angle Φ can be found by considering the equation for the amplitude, B, of the second roll, (2.15*b*). On linearizing (2.15*b*) with respect to B, where A is given by (3.2), setting $B = \exp(\lambda\tau + iLX_b)$ and maximizing the growth rate with respect to L and Φ, it is found that the most unstable mode of this form has wavenumber k_c, corresponding to $L = 0$, and is perpendicular to the basic roll. The marginal stability curve is given by

$$\tfrac{40}{3}K^2 = R_{cr} + k_c^3 (20/3)(10/7)^{\frac{1}{2}} R_{cr}^{-\frac{1}{2}}, \tag{3.4}$$

which is labelled (*a*) in figure 2. A curve of this form has been presented by Vozovoi & Nepomnyaschii (1974) for the corresponding Bénard problem. It is pertinent to note that as R_{cr} increases, the second term on the right-hand side of (3.4) tends to zero and we recover the stability curve for the Lapwood (1948) problem, $R_{cr} = \frac{40}{3}K^2$.

The evolution of this instability has been analysed by Rees & Riley (1986) for the related problem of undulating isothermal boundaries, and the details are therefore omitted here. To summarize: there are two stable solutions, namely, the basic roll and a mixed mode, which is a linear superposition of a weakened basic roll and the fully evolved cross-roll disturbance. The results are represented in the form of

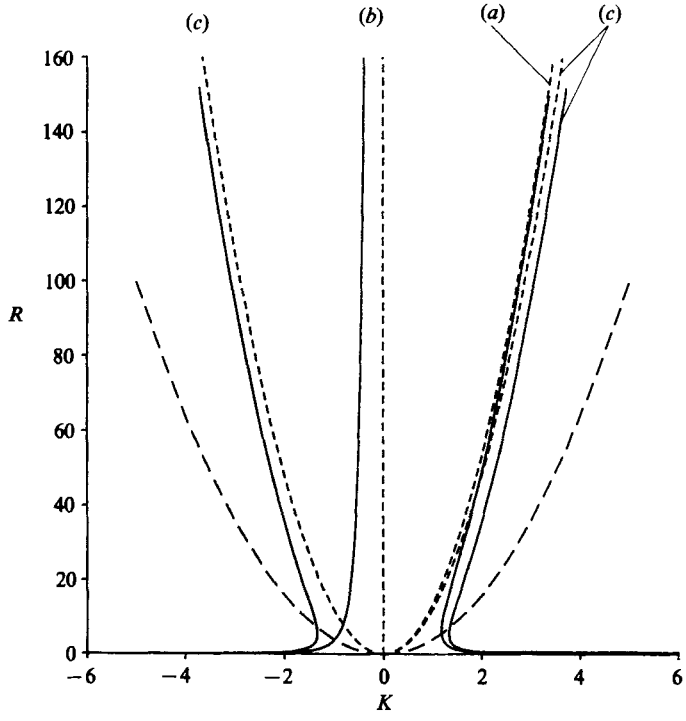

FIGURE 2. Marginal stability curves for the (*a*) cross-roll, (*b*) zigzag, and (*c*) sideband instabilities. ——, with thermal noise; – – – –, without thermal noise; — — — —, marginal stability curve for the onset of Lapwood convection.

bifurcation diagrams in figure 3. For large detuning ($|K|$ large), there are two symmetry-breaking bifurcations off the pure A-mode solution branch, with the basic roll unstable over a finite continuous range of Rayleigh number, (*a*). As the detuning decreases the leading branches develop quartic contact and then the bifurcation goes subcritical, (*b*). The two bifurcation points eventually become coincident, (*c*), and the mixed-mode branches then disconnect in the opposite sense. This process leaves the pure A-mode completely stable to cross-roll disturbances, and each of the disconnected mixed-mode solution branches have a stable and an unstable branch, (*d*). The critical values of K at which these two events occur are given in Rees & Riley (1986).

4. The zigzag instability for the sinuous configuration

The linear stability of the basic roll to zigzag disturbances may be considered (cf. Newell & Whitehead 1969) by substituting $A = (A_0+\alpha)\exp(\mathrm{i}KX)$ in (2.13) and linearizing with respect to α. Setting

$$\alpha = (\alpha_1 \mathrm{e}^{\mathrm{i}(LX+MY)} + \alpha_{-1}\mathrm{e}^{-\mathrm{i}(LX+MY)})\,\mathrm{e}^{\lambda\tau}, \tag{4.1}$$

and maximizing λ with respect to L and M yields the three relative maxima: (i) $L = M = 0$ which leads to the result of §3 that the secondary branches of the basic roll solution are unstable: (ii) $M = 0$ and $L^2 = K^2 - k_c^8 A_0^4/64K^2$ which yields the sideband instability to be considered in §5; and (iii) $L = 0$ and $M^2 = -2k_cK$, the

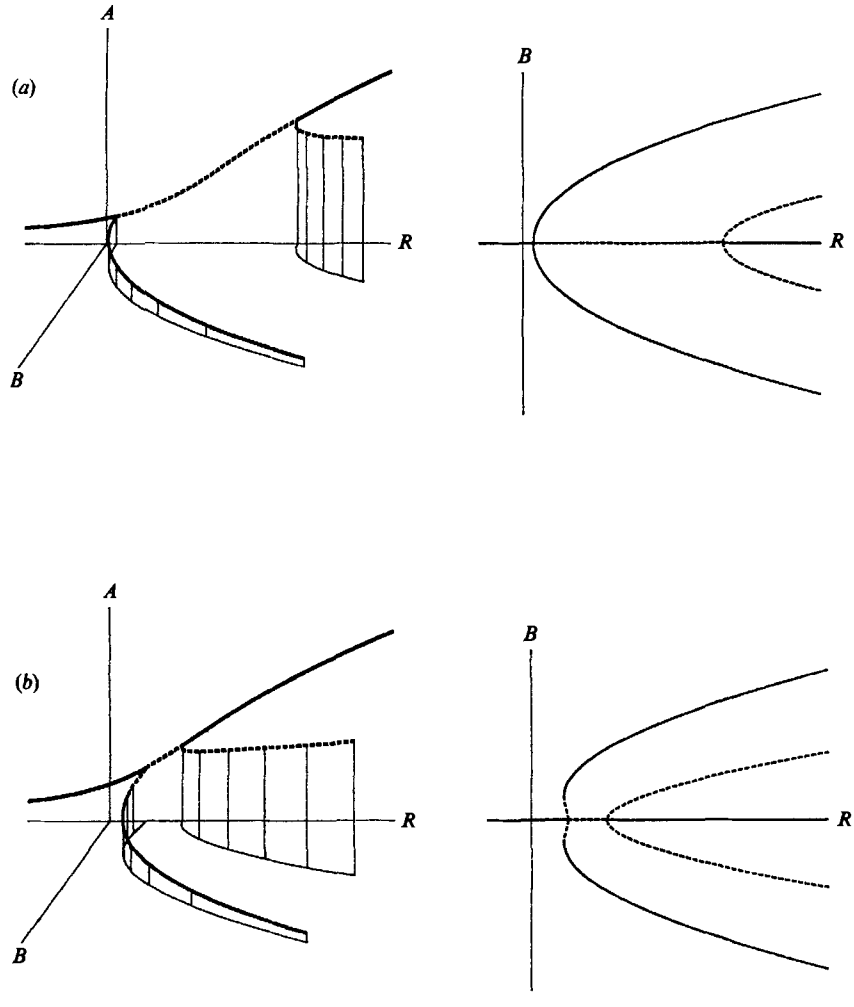

FIGURE 3(a, b). For caption see facing page.

zigzag instability which exists when K is negative, i.e. for rolls with lengthscale larger than the critical Lapwood roll. It is easily shown that the marginal stability curve for zigzag disturbances is given by

$$R_z = \tfrac{1}{4}k_c^6 K^{-4}, \quad K < 0, \tag{4.2}$$

which is labelled (*b*) in figure 2. Roll solutions to the left of this curve are unstable and it is interesting to note that the unstable mode has the form $\alpha_1 = -\bar{\alpha}_{-1}$ corresponding to the sinuous zigzag instability (cf. Joseph 1976). The corresponding curve for the Bénard problem is again given in Vozovoi & Nepomnyaschii (1974).

In order to make analytical progress in considering the evolution of the unstable flow, weakly nonlinear theory is used. Assuming that (R, K) is close to the neutral curve, A and R are expanded as follows:

$$R = R_z(K) + \beta^2 R_2 + \ldots, \tag{4.3a}$$

$$A = (A_0 + \beta A_1 + \beta^2 A_2 + \ldots)\, e^{iKX}, \tag{4.3b}$$

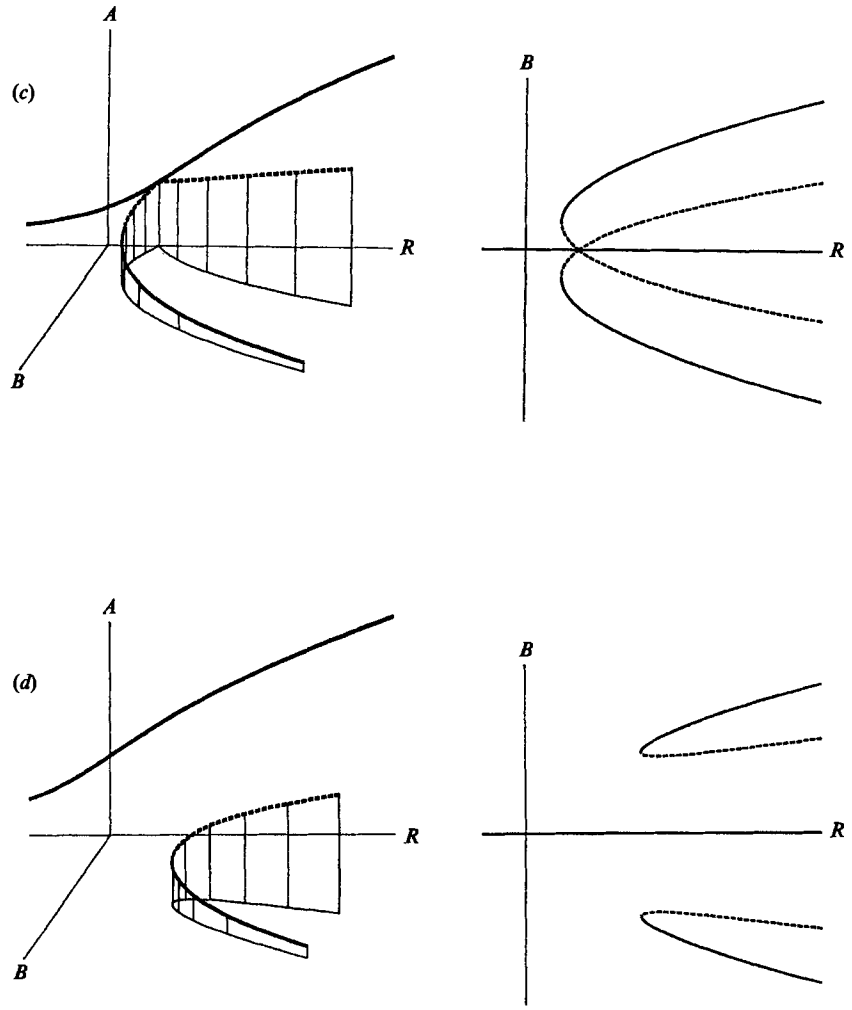

FIGURE 3. Sketches of the bifurcation diagrams for the cross-roll instability for decreasing values of $|K|$. The axes labelled A and B represent the modal amplitudes as in (3.4). Solid lines represent stable modes, and dashed lines unstable modes.

where $\beta \ll 1$, $R_z(K)$ lies on the neutral curve, A_0 is given by (3.3), and

$$A_1 = \gamma e^{iMY} - \bar{\gamma} e^{-iMY}, \tag{4.4}$$

where $\gamma = \gamma(\tau^*)$, $\tau^* = \beta^2\tau$ is a slow timescale, and $M = (-2k_c K)^{\frac{1}{2}}$. At $O(\beta^3)$, a solution exists only if

$$\frac{d\gamma}{d\tau^*} = \left[\frac{R_2\gamma}{1+k_c^3 A_0^3} - \left(\frac{16K^{12}+36K^6k_c^6+k_c^{12}}{576K^{12}+80K^6k_c^6+k_c^{12}}\right)\gamma^2\bar{\gamma}\right], \tag{4.5}$$

which implies that the bifurcation is supercritical at all points on the curve.

At points further away from the neutral curve it becomes necessary to solve the fully nonlinear equation. To effect the solution we use a Galerkin method and expand the amplitude as follows:

$$A = \sum_{n=-N}^{N} B_n(\tau)\, e^{i(KX+nMY)}, \tag{4.6}$$

where N is the truncation level of the series. It is important to note that we have assumed that the wavenumber modulation in the X-direction is due solely to the boundary forcing: this corresponds to suppressing the sideband instability. The coefficients B_n satisfy

$$\frac{\mathrm{d}}{\mathrm{d}\tau}(B_n) = \left[R - \left(2K + \frac{n^2M^2}{k_c}\right)^2\right]B_n - k_c^4 C_n + 2k_c\,\delta_{0n}, \quad n = -N, \ldots, N, \tag{4.7}$$

where $\delta_{0n} = 1$ if $n = 0$ and is zero otherwise, and

$$C_n = \sum_{m=-2N}^{2N} \sum_{p=-N}^{N} B_{n-m}\, B_p\, \bar{B}_{p-m}, \tag{4.8}$$

with $B_q \equiv 0$ for $|q| > N$. Equations (4.7) are readily solved using the NAG library initial-value ordinary differential equation solver D02BBF. This method was chosen in order to ascertain the effects of initial conditions on the resulting steady solutions. The results we present are in the form of graphs of the quantities B_z and ϕ_z defined by

$$B_z = \left[\left(\sum_{n=-N}^{N} \mathscr{B}_n \cos\left(nM(Y+\alpha_n)\right)\right)^2 + \left(\sum_{n=-N}^{N} \mathscr{B}_n \sin\left(nM(Y+\alpha_n)\right)\right)^2\right]^{\frac{1}{2}}, \tag{4.9}$$

$$\cos\phi_z = \left(\sum_{n=-N}^{N} \mathscr{B}_n \cos\left(nM(Y+\alpha_n)\right)\right) \Big/ B_z, \tag{4.10}$$

$$\sin\phi_z = \left(\sum_{n=-N}^{N} \mathscr{B}_n \sin\left(nM(Y+\alpha_n)\right)\right) \Big/ B_z, \tag{4.11}$$

where $B_n = \mathscr{B}_n \mathrm{e}^{\mathrm{i}nM\alpha_n}$, and $\mathscr{B}_n$ is real and positive. The x-component of the fluid velocity in the layer is proportional to $B_z \cos\left(k_c x + KX + \phi_z(Y)\right)$. Thus if we define the cell boundaries to be the surfaces where there is no flow in the x-direction then these boundaries occur at

$$k_c x + KX + \phi_z(Y) = (\hat{n} + \tfrac{1}{2})\pi, \tag{4.12}$$

for integer $\hat{n}$, and the local wavevector of the rolls is given by

$$\left(k_c + \epsilon^{\frac{1}{3}}K,\ \epsilon^{\frac{1}{6}}\frac{\partial}{\partial Y}(\phi_z)\right). \tag{4.13}$$

Thus B_z is the local amplitude of the rolls as a function of Y, and ϕ_z represents the shape of the roll axis.

The numerical computations suggest that there are three stable steady solutions, namely, the basic roll and two others, which we label types I and II. We infer from these calculations that the bifurcation diagrams corresponding to the zigzag instability are as sketched in figure 4. If R is considered to be constant, then the basic roll is linearly stable for small positive values of $-K$ and all $K > 0$. When K is given by (4.2) there is a supercritical bifurcation to the weakly nonlinear solution given above, which we label type I. In figure 5 values of B_z and ϕ_z are displayed for a steady solution with $(R, K) = (10, -1)$, a type-I solution, which is typical of those found just within the unstable region. In this case we found that a truncation level $N = 6$ gives a sufficiently accurate solution. The integration may be initiated either by using the basic roll solution (i.e. taking $B_0(0) = A_0$) together with small values of $B_1 = -\bar{B}_{-1}$ so that the evolution can be followed in time, or by using large values of $B_1 = -\bar{B}_{-1}$ in order to decrease the integration time. From the ϕ_z plot it can be seen that the roll axis of this solution is not straight, but exhibits a spatially periodic

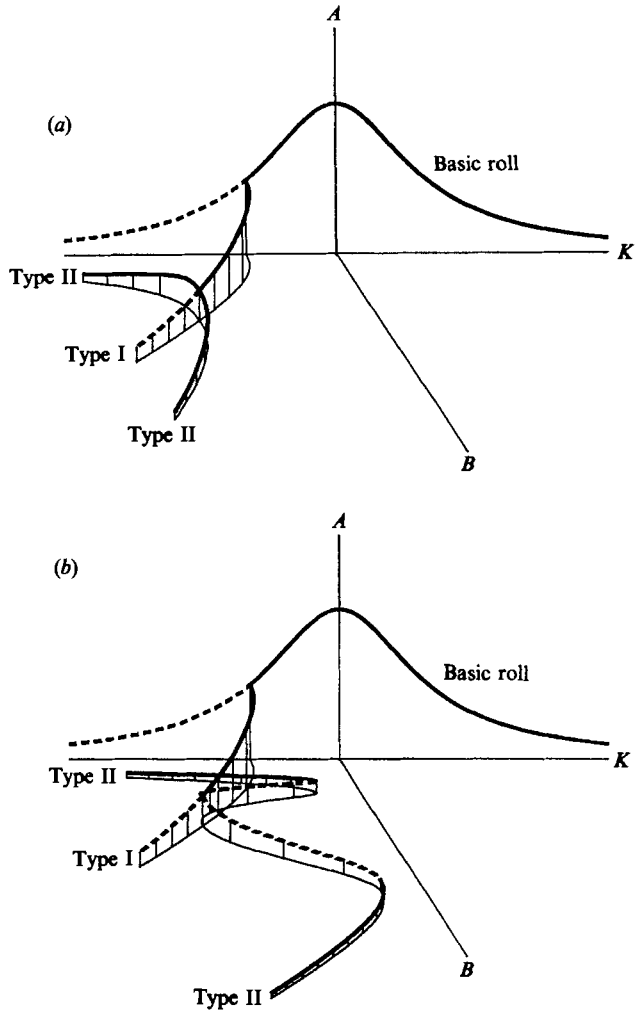

FIGURE 4. Sketches of the bifurcation diagrams for the zigzag instability: (*a*) $R < 3.3$, and (*b*) $R > 3.3$. Here A represents the amplitude of the basic-roll component, B_0, and B is a measure of the strength of the zigzag components, e.g. $|B_1|$ or $|B_{-1}|$.

deviation about the axis of the basic roll, $\phi_z = 0$. This solution has the same form as the weakly nonlinear solution derived earlier.

For larger values of $-K$ the amplitude of ϕ_z increases so that the roll axis exhibits increasingly larger deviations from a straight line. At a second critical value of K (the first being the neutral curve) the type-I solution, for which $B_1 = -\bar{B}_{-1}$, becomes unstable to small perturbations of the form $B_1 = \bar{B}_{-1}$. The subsequent evolution is such that the final steady solution has either B_1 or B_{-1} dominating; it is this solution we label type II. A typical example of this solution, for which (R, K) is again $(10, -1)$, is shown in figure 6 where we see that the rolls are aligned away from the basic-roll axis in the mean. For this solution the axial deviation from straight line decreases as we recede from the neutral curve, which is to be expected since large values of $-K$ imply a weak basic flow. This secondary bifurcation may be either supercritical or subcritical depending on the precise value of R. If we fix R and vary K, then the bifurcation is subcritical when $R > 3.3$ and supercritical otherwise.

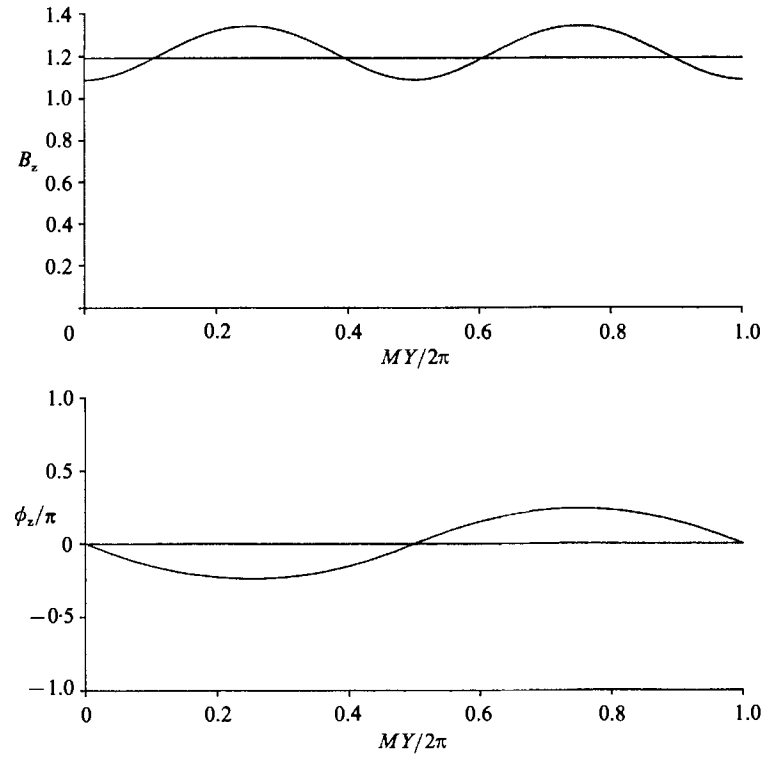

FIGURE 5. A steady solution for the zigzag instability for $R = 10, K = -1$ and M given by its critical value. This type-I solution is typical for (R, K) close to the neutral curve. The constant solution corresponds to the basic roll.

Numerically we have found that the degree of subcriticality can be such that it is possible to obtain type-II solutions well within the linearly stable region and even for positive values of K. The plan views of both types I and II solutions are sketched in figure 7 together with the basic roll for comparison.

5. The sideband instability for the sinuous configuration

For the Bénard problem it is well known (Newell & Whitehead 1969) that a roll may become unstable to two-dimensional disturbances; we now investigate how the presence of boundary imperfections modify this instability in the case of Lapwood convection. As mentioned earlier, such an instability may arise if the layer is finite in the y-direction, of width W, say. In particular, it is necessary that (i) $W = o(\epsilon^{-\frac{1}{6}})$, so that the zigzag instability cannot be accommodated within the layer, and (ii) W is not too close to $2\pi N^*/k_c$ for any integer N^*, so that transverse rolls with wavenumber $k_c + O(\epsilon^{\frac{1}{3}})$ cannot fit into the layer. Mathematically, these conditions can be made more precise by setting $W = 2\pi N^*/k_c + \delta$, where the integer $N^* = O(\epsilon^{-a})$ and $\delta = O(\epsilon^b)$, to give the requirements, $0 < a < \frac{1}{6}$ and $0 < b < \frac{1}{3} - a$. As noted earlier the present analysis is also important in studying the stability of convection in a long Hele-Shaw cell.

The appropriate amplitude equation is again given by (3.1) and the linear stability

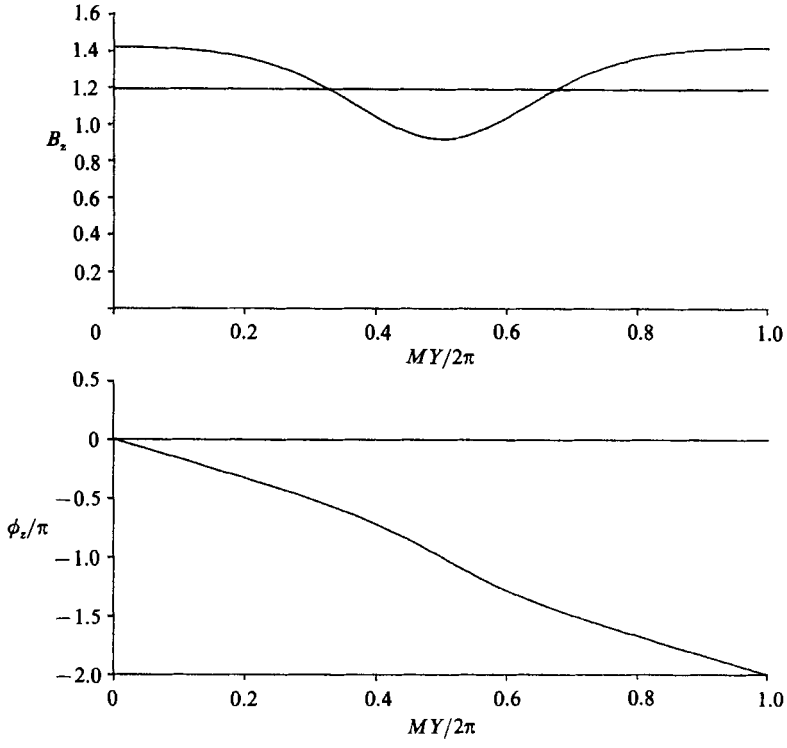

FIGURE 6. A steady solution for the zigzag instability for $R = 10$, $K = -1$ and M given by its critical value. This type-II solution is typical for (R, K) far from the neutral curve. The constant solution corresponds to the basic roll.

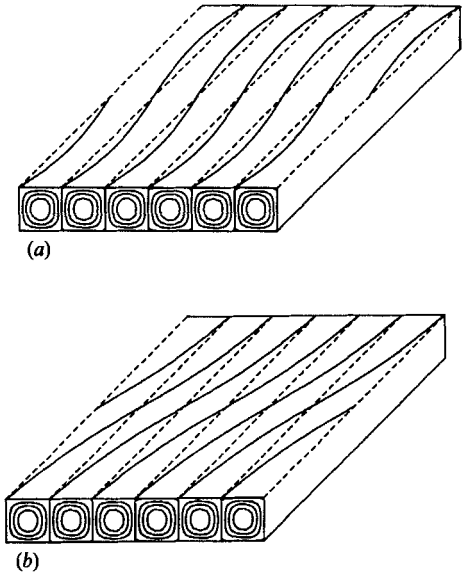

FIGURE 7. A sketch of the cellular structures corresponding to solutions of (*a*) type I, (*b*) type II. The dashed lines represent the alignment of the basic roll.

of the basic flow is considered by substituting $A = (A_0+\eta)\exp(\mathrm{i}KX)$ in (3.1) and linearizing with respect to η. On setting

$$\eta = (\eta_1 \mathrm{e}^{\mathrm{i}LX} + \eta_{-1}\mathrm{e}^{-\mathrm{i}LX})\,\mathrm{e}^{\lambda\tau} \tag{5.1}$$

it is found that the growth rate, λ, is maximized when $L^2 = K^2 - k_c^8 A_0^4/64K^2$. The marginal stability curve, found by setting $\lambda = 0$, is labelled (*c*) in figure 2. We note that it lies entirely within the unstable region of the cross-roll instability and is therefore less important in a fully three-dimensional context. In the present case, the most unstable mode has $\eta_1 = c\bar{\eta}_{-1}$, where c is a real function of R_s, and where $R_s = R_s(K)$ lies on the sideband neutral curve.

To consider the nature of the bifurcation corresponding to points on the neutral curve, we proceed as for the zigzag instability by performing a weakly nonlinear analysis using (4.3) with R_z replaced by R_s, and $A_1 = A(\tau^*)(c\,\mathrm{e}^{\mathrm{i}LX} + \mathrm{e}^{-\mathrm{i}LX})$ where A is complex, in general. Again, at $O(\beta^3)$, a solution exists only if

$$\frac{\mathrm{d}A}{\mathrm{d}\tau^*} = R_2\mu_1 A + \mu_2 A^2\bar{A}, \tag{5.2}$$

where μ_1 and μ_2 are real constants. It is found that $R_2\mu_1$ is positive to the right of the neutral curve for $K > 0$, which is in agreement with the linear theory. The bifurcation is subcritical when $\mu_2 > 0$, which holds when $R_s > 7.308\,75$.

The nonlinear evolution of the sideband disturbances may be followed by again using a Galerkin method. Expanding A in the form

$$A = \sum_{n=-N}^{N} B_n(\tau)\,\mathrm{e}^{\mathrm{i}(nL+K)X}, \tag{5.3}$$

where L is not necessarily equal to the maximizing value given above, yields the equations

$$\frac{\mathrm{d}}{\mathrm{d}\tau}(B_n) = [R - 4(nL+K)^2]B_n - k_c^4 C_n + 2k_c\,\delta_{0n}, \quad n = -N,\ldots,N, \tag{5.4}$$

where C_n is given by (4.8).

The results are presented in terms of B_s and ϕ_s, where

$$B_s = \left[\left(\sum_{n=-N}^{N} \mathscr{B}_n \cos(nL(X+\alpha_n))\right)^2 + \sum_{n=-N}^{N} \mathscr{B}_n \sin(nL(X+\alpha_n))\right)^2\Bigg]^{\frac{1}{2}}, \tag{5.5}$$

$$\cos\phi_s = \left(\sum_{n=-N}^{N} \mathscr{B}_n \cos(nL(X+\alpha_n))\right)\Big/ B_s, \tag{5.6}$$

$$\sin\phi_s = \left(\sum_{n=-N}^{N} \mathscr{B}_n \sin(nL(X+\alpha_n))\right)\Big/ B_s, \tag{5.7}$$

where $\mathscr{B}_n$ is defined as in §4. The roll stream function (cf. Rees & Riley 1986), ψ, is given by

$$\psi = 2k_c B_s(X)\cos(k_c x + KX + \phi_s(X)), \tag{5.8}$$

so that B_s measures the local roll amplitude and ϕ_s the local phase of the rolls relative to the boundary forcing. The local roll wavenumber is now given by

$$k_s = k_c + \epsilon^{\frac{1}{3}}\left(K + \frac{\mathrm{d}}{\mathrm{d}X}(\phi_s)\right). \tag{5.9}$$

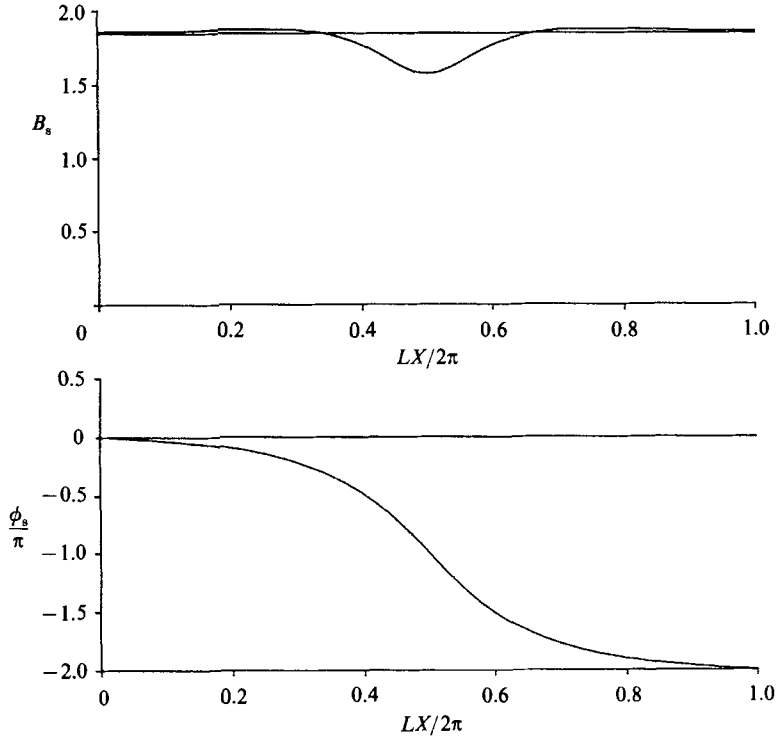

FIGURE 8. Steady solutions for the sideband instability for $R = 20$, $K = L = 0.5$. The constant solution is the (linearly stable) basic roll.

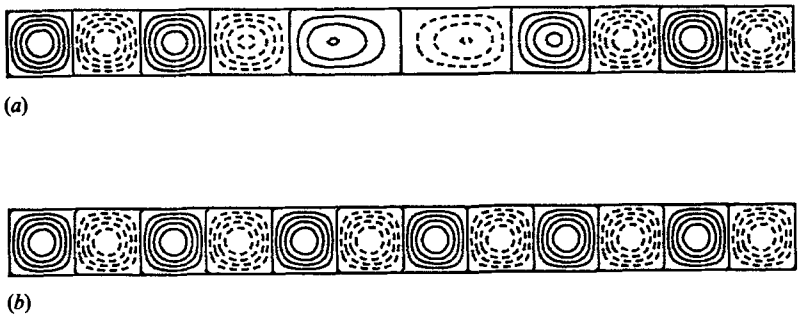

FIGURE 9. A sketch of typical streamlines for (*a*) a sideband dominated solution, and, for comparison, (*b*) the basic roll. The phase of the basic roll is such that there is no horizontal flow at stations where the boundary temperatures take maximum or minimum values.

The findings above regarding the nature of the bifurcation at the marginal curve have been confirmed using the numerical scheme. In figure 8, B_s and ϕ_s are shown for $(R, K) = (20, 0.5)$ with $L = 0.5$ – a parameter case where the basic roll is linearly stable. This solution was obtained by introducing a large sideband perturbation to the basic-roll solution, and using a truncation level $N = 9$. Over a length of $2\pi/L$ in the X-direction this solution has two fewer cells than the basic roll; this is seen clearly in figure 9 where typical streamlines for a fully evolved sideband disturbance are displayed. In figures 8 and 9 it is seen that at $X = \pi/L$, the roll phase is $\phi_s = -\pi$, which corresponds to flow in a direction opposing the buoyancy forces. Consequently

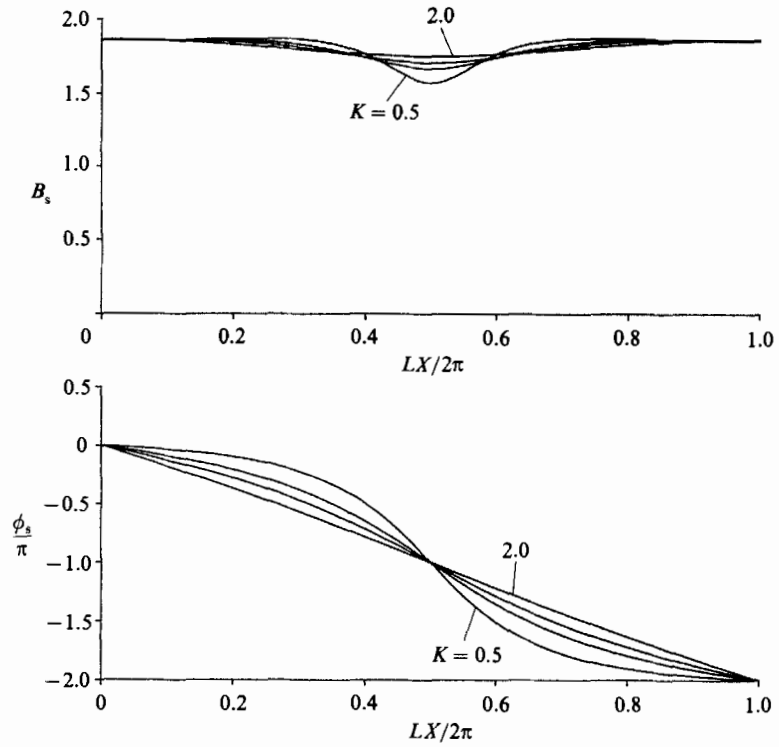

FIGURE 10. The effect of different values of K and L on the steady solutions for the sideband instability: $R = 20$ and $K = L = 0.5$, 0.75, 1.0, and 2.0.

there is a local decrease in the roll amplitude. In figure 10 we display various solutions, again for $R = 20$, but with $K = L = 0.5$, 0.75, 1.0 and 2.0. Here we see that as K increases the computed solution tends towards a solution with a constant wavenumber. This is a consequence of the decreasing strength of the basic flow, which has a diminishing effect on the final solution as K becomes large. The bifurcation diagrams corresponding to our analytical and numerical results for the sideband instability were found to be qualitatively the same as for the cross-roll instability, shown in figure 3. The axis labelled B in figure 3 is to be interpreted here as some measure of the magnitude of the sideband components, such as $|B_{-1}|$ if $K > 0$, or $|B_1|$ for $K < 0$.

6. The sideband instability for the varicose configuration

Finally, we turn our attention to the two-dimensional stability of rolls in a layer with near-resonant varicose thermal forcing. As mentioned in the introduction this is of relevance when considering a shallow Hele-Shaw cell or a porous layer which is narrow in the y-direction (i.e. the layer is sufficiently restricted that the rectangular cells described in Rees & Riley (1988) cannot fit into the layer).

The governing amplitude equation (2.18) may be reduced to a canonical form by introducing the substitutions

$$A = \frac{I_5^{\frac{1}{2}} A^+}{k_c^2}, \quad R = R_2^+ I_5 + I_4, \quad X = \frac{X^+}{I_5^{\frac{1}{2}}}, \quad K = K^+ I_5^{\frac{1}{2}}, \quad \tau = \frac{\tau^+}{I_5}, \tag{6.1}$$

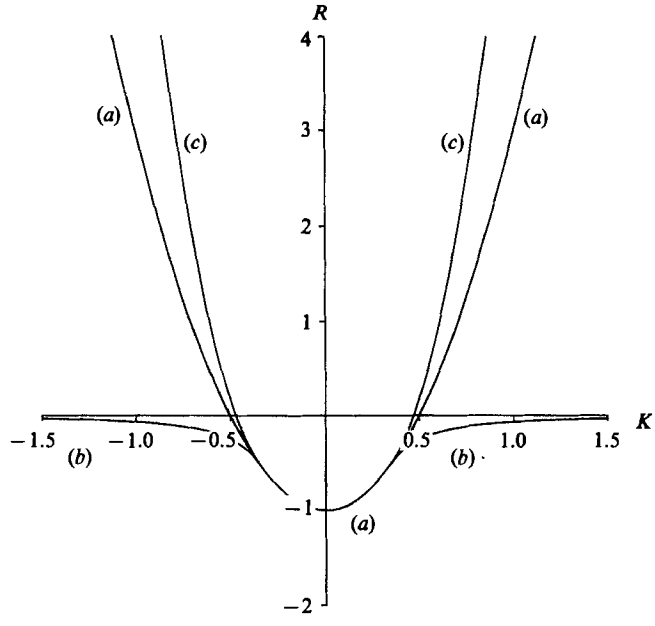

FIGURE 11. Marginal stability curves for the layer with varicose heating: (*a*) onset of the single mode, (*b*) onset of multiple-roll flow (instability of zero solution), (*c*) instability of the single roll to sideband disturbances.

which, on omitting the superscripts, yield

$$A_\tau = RA + \bar{A}\,\mathrm{e}^{2\mathrm{i}KX} + 4A_{XX} - A^2\bar{A}. \tag{6.2}$$

It is interesting to contrast the natures of the sinuous and varicose thermal forcing by comparing the respective amplitude equations (3.1) and (6.2). In the former case an inhomogeneous spatially varying term appears, thus causing all possible solutions to contain a component proportional to $\mathrm{e}^{\mathrm{i}KX}$. In the latter case the forcing manifests itself as a variable coefficient so that it is possible to have not only the zero solution but also solutions without a component proportional to $\mathrm{e}^{\mathrm{i}KX}$.

The stability of the $A = 0$ solution may now be determined. Consider first the stability with respect to disturbances with spatial form $\mathrm{e}^{\mathrm{i}KX}$. On setting $A = \alpha(\tau)\mathrm{e}^{\mathrm{i}KX}$ in (6.2) and linearizing with respect to α we obtain

$$\alpha_\tau = (R - 4K^2)\alpha + \bar{\alpha}, \tag{6.3}$$

from which we deduce that there are two normal modes for which α is either real or imaginary. Thus the critical values of R, R_{vr} and R_{vi} above which these respective modes grow are given by

$$R_{\mathrm{vr}} = 4K^2 - 1, \qquad R_{\mathrm{vi}} = 4K^2 + 1. \tag{6.4a, b}$$

These respective modes correspond to the type I and II modes described in Rees & Riley (1986). It is an easy matter to show that the type-II solution is unstable to phase disturbances. The marginal stability curve (6.4*a*) is plotted in figure 11 and labelled (*a*).

As pointed out by Newell & Whitehead (1969) a mode consisting of a pair of rolls may also bifurcate from the trivial solution – the analysis follows as in §5. Thus we set

$$A = (\alpha_1\,\mathrm{e}^{\mathrm{i}LX} + \alpha_2\,\mathrm{e}^{-\mathrm{i}LX})\,\mathrm{e}^{\mathrm{i}KX + \lambda\tau} \tag{6.5}$$

in (6.2) and linearize with respect to α_1 and α_2. This disturbance has growth rate

$$\lambda = R - 4(K^2 + L^2) + (64K^2L^2 + 1)^{\frac{1}{2}}, \tag{6.6}$$

from which we deduce that the maximum growth rate occurs when $L = L_{c0}$, where

$$L_{c0}^2 = (K^4 - \tfrac{1}{64})^{\frac{1}{2}}/K^2, \tag{6.7}$$

and is given by

$$\lambda_{\max} = R_2 + 1/16K^2. \tag{6.8}$$

Hence the critical curve for these disturbances is given by

$$R = -1/16K^2, \tag{6.9}$$

which is subject to $K^2 > \frac{1}{8}$ (from (6.7)), and is plotted in figure 11 and labelled (*b*). For values of K^2 less than $\frac{1}{8}$, λ is maximized when $L = 0$ and the above single-mode analysis becomes appropriate. It is pertinent to note that $\alpha_1/\alpha_2 \to 0$ and $L_{c0} \to K$ as $K \to \infty$, and therefore, in this case, the most dangerous mode consists of a single roll whose wavenumber $k_c + (K - L)\epsilon \to k_c$ as $K \to \infty$. In this way the results of Rees & Riley (1989) are recovered for the onset of finite-amplitude convection in the form of longitudinal rolls with wavenumber k_c where the varicose thermal forcing has wavenumber k_w and $k_w \to k_c$.

We now consider the stability of the finite-amplitude single-roll solution, $A = (R + 1 - 4K^2)^{\frac{1}{2}} e^{iKX}$, to sideband disturbances. Let

$$A = [(R + 1 - 4K^2)^{\frac{1}{2}} + \eta] e^{iKX}, \tag{6.10}$$

in (6.2) and linearize with respect to η. The maximum growth rate for the disturbances occurs when $L = L_{c1}$, where

$$L_{c1}^2 = K^2 - (R - 4K^2)^2/64K^2 \tag{6.11}$$

and is given by

$$\lambda_{\max} = (R - 4K^2)^2/16K^2 - (R - 4K^2) + (4K^2 - 2). \tag{6.12}$$

In general $L_{c0} \neq L_{c1}$ and therefore the wavenumber of the most dangerous sideband disturbance depends on the initial flow. The critical curve is easily determined to be

$$R = 12K^2 - 4\sqrt{2}K, \tag{6.13}$$

which is shown in figure 11 and labelled (*c*). The qualitative features of figure 11 also appear in Wynne (1987). It is of interest to note that the marginal stability curves (6.4*a*), (6.9) and (6.13) are not only coincident at $(R, K) = (-\frac{1}{2}, \pm 1/\sqrt{8})$, but have identical tangents at that point. A weakly nonlinear analysis of the bifurcation at points on the curve given by (6.13) reveals that it is supercritical as R increases.

Once more we follow the evolution of the sideband instability using the Galerkin scheme derived earlier. For the remainder of this section the notation of §5 will be employed. For this configuration the amplitudes of the various roll components B_n (cf. (5.3)) satisfy the following set of equations:

$$\frac{\mathrm{d}}{\mathrm{d}\tau}(B_n) = [R - 4(nL + K)^2] B_n + B_{-n} - 4k_c^4 C_n, \quad n = -N, \ldots, N. \tag{6.14}$$

The results derived earlier have been confirmed using the numerical scheme. It appears that there are two types of solution to (6.14) that are stable: the first corresponds to the finite-amplitude single-mode solution $A = (R + 1 - 4K^2)^{\frac{1}{2}} e^{iKX}$, and

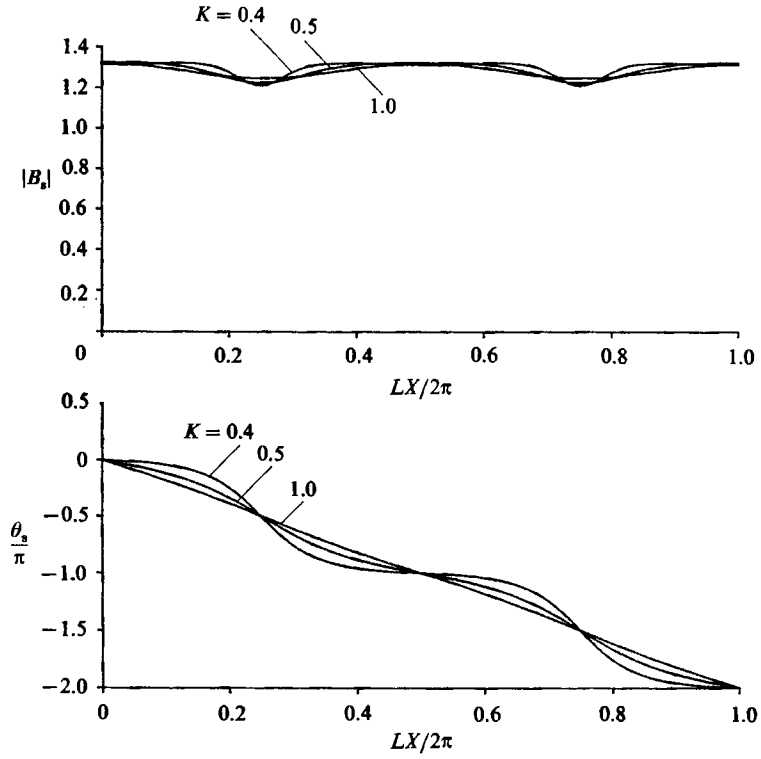

FIGURE 12. Steady solutions for the sideband instability with varicose heating for $R = 10$, $K = 0.4$, 0.5, 1.0, and $L = L_{c0}(K)$.

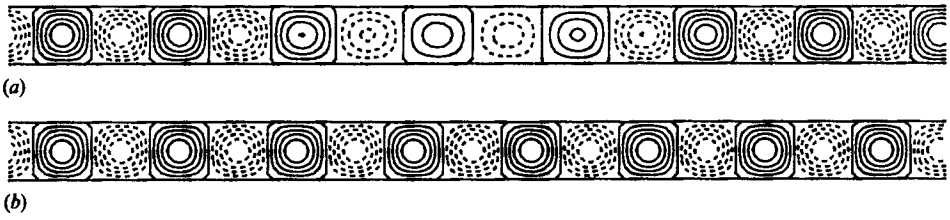

FIGURE 13. A sketch of the cellular structures corresponding to (*a*) a multiple-roll flow, (*b*) the single roll. The phase of the single roll is such that the horizontal velocity is zero at stations where the temperature difference across the layer takes its mean value.

the second is a superposition of modes with wavenumbers $k_c + (K + (2n+1)\,L)\,\epsilon$. This latter solution does not contain a mode with the forcing wavenumber $k_w = k_c + \epsilon K$. We show typical examples of this solution in figure 12 where B_s and ϕ_s are plotted for the cases $R = 10$, $K = 0.4$, 0.5, and 1.0, $L = L_{c0}(K)$ and $N = 9$. It is evident from figure 12 that when K is small the local phase of the flow is close to $n\pi$ for a large part of the interval $X = 0$ to $X = 2\pi L$, with a relatively small region where the phase undergoes a transition from $n\pi$ to $(n-1)\,\pi$. This transition is accompanied by a local reduction in the amplitude B_s. This is illustrated in figure 13 where we show typical streamlines for such a solution. For larger values of K the slope of the phase plot tends more towards a constant value, indicating that one mode (i.e. the one with wavenumber $k_c + (K - L)\,\epsilon$) dominates all the others.

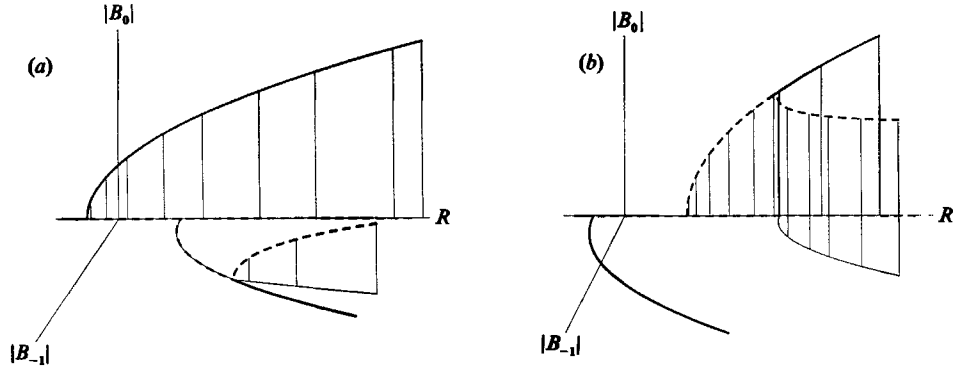

FIGURE 14. Sketches of the bifurcation diagrams for the sideband instability for varicose heating for (*a*) small positive K, (*b*) large positive K. For negative K replace $|B_{-1}|$ by $|B_1|$.

In figure 14 we show sketches of the bifurcation diagrams corresponding to the stable solutions which have been determined numerically, and the unstable solutions whose presence we have inferred from elementary bifurcation theory. For $K^2 < \frac{1}{8}$ the first mode to bifurcate from the trivial solution is the single-roll solution, and corresponds to $L = 0$. At higher values of R multiple-mode solutions ($L \neq 0$) bifurcate from the zero solution, but are initially unstable. At still larger values of R stable multiple-mode solutions exist, and therefore we infer the presence of an unstable mixed single- and multiple-mode solution as shown in figure 14(*a*). For larger values of K = the multiple-mode solution occurs first as R is increased, as seen in figure 14(*b*). As R is increased further the single-mode solution bifurcates supercritically from the zero solution, but this is unstable until a secondary bifurcation to an unstable multiple mode. A difficulty arises at this point since, if the flow corresponded to a stable point on the single-mode branch, and R were reduced past the secondary bifurcation point, then the flow would evolve to a multiple-mode state different from that obtained by increasing R to the same value. This is a consequence of the fact that the critical value of the sideband wavenumber, L, differs in different circumstances. In general it would seem likely that the flow obtained at particular values of R and K will depend on the past history.

7. Conclusions

We have studied the stability of rolls and the evolution of instabilities in a saturated porous layer when the temperatures of both horizontal boundaries vary periodically in one direction about their respective mean values. Attention has been focused on the effect of small-amplitude modulations, with wavenumber close to k_c, on convective rolls for Rayleigh numbers near Ra_c.

The marginal curves for cross-roll, zigzag and sideband instabilities for a sinuous modulation have been calculated and it has been shown that the region of linear stability of the basic two-dimensional flow is enlarged by the presence of the modulation.

When the basic roll in the sinuously heated layer is unstable to the zigzag instability, the roll axis deforms and exhibits spatially periodic deviations about its original direction; this solution occurs when (Ra, k_w) is close to the neutral curve. Further away from the curve this solution becomes unstable and evolves to a roll

whose axis has spatially periodic deviations about a direction inclined at a small angle to the basic roll. When the basic roll is unstable to the sideband instability the ultimate steady flow (in the absence of other types of disturbance) is a roll with a spatially periodic amplitude and phase. Thus the zigzag and sideband instabilities give rise to a number of novel roll patterns, which, as far as we know, have not yet been observed in experiments.

We have concentrated on the effects of each instability in isolation but, in general, all three could exist at any one time. Although further work needs to be done on this aspect, we believe that the fully evolved solutions presented here are the only possible solutions in an unbounded layer. It is also likely that some solutions assumed to be stable here are unstable, e.g. the 'stable' solutions near the limit point in figure 4(*b*) may be unstable to sideband or cross-roll disturbances.

For heating with a varicose modulation, we considered two-dimensional flows and analysed the sideband instability only. In general, a more important three-dimensional instability does exist, but we assumed that conditions were such that it could be ignored. It was found that, owing to the modulations, the onset of rolls occurs at a lower Rayleigh number and the destabilization due to the sideband instability is delayed. When there is a large detuning of the modulation wavenumber away from k_c (but still within an $O(\epsilon)$ range) the first mode to appear as the Rayleigh number increases consists of a pair of rolls. The ultimate steady flow that arises from the sideband instability is again a roll with a spatially periodic amplitude and phase. However the wavenumber of the most dangerous sideband disturbance depends on the past history of the flow unlike the case of a sinuously heated layer.

We have concentrated on one-dimensional imperfections and it is natural to question what would the effects be of two or more modes with non-parallel wavevectors and different wavenumbers. Although this is outside the scope of this paper much may be deduced about the flow patterns with little analysis. A good example is the case of two modes with perpendicular wavevectors and equal wavenumbers close to k_c. In this case the flow occurring subcritically consists of square cells which persist until they become unstable at $Ra = Ra_c + O(\delta^{\frac{2}{3}})$ to form a pair of rolls with unequal amplitudes. As $(Ra - Ra_c)/\delta^{\frac{2}{3}}$ increases one of the rolls decays to zero recovering the result of the perfect problem that rolls are the only stable mode. The precise quantitative results require a similar analysis to that presented in this paper.

One of us (D.A.S.R.) wishes to thank the S.E.R.C. for support under Research Grant GR/D/46601. The authors wish to thank the referees for constructive criticism on the preparation of this paper.

REFERENCES

Bolton, E. W., Busse, F. H. & Clever, R. M. 1986 Oscillatory instabilities of convection rolls at intermediate Prandtl numbers. *J. Fluid Mech.* **164**, 469–485.

Busse, F. H. & Clever, R. M. 1979 Instabilities of convection rolls in a fluid of moderate Prandtl number. *J. Fluid Mech.* **91**, 319–335.

Busse, F. H. & Whitehead, J. A. 1971 Instability of convective rolls in a high Prandtl number fluid. *J. Fluid Mech.* **47**, 305–320.

Busse, F. H. & Whitehead, J. A. 1974 Oscillatory and collective instabilities in large Prandtl number convection. *J. Fluid Mech.* **66**, 67–79.

Coullet, P. 1987 Commensurate–incommensurate transitions in nonequilibrium systems. *Phys. Rev. Lett.* **56**, 724–727.

DANIELS, P. G. 1982 Effects of geometrical imperfection at the onset of convection in a shallow two-dimensional cavity. *Intl J. Heat Mass Transfer* **25**, 337–343.

EAGLES, P. M. 1980 A Bénard convection problem with a perturbed lower wall. *Proc. R. Soc. Lond.* A **371**, 359–379.

HALL, P. & WALTON, I. C. 1977 The smooth transition to a convective régime in a two-dimensional box. *Proc. R. Soc. Lond.* A **358**, 199–221.

HALL, P. & WALTON, I. C. 1979 Bénard convection in a finite box: secondary and imperfect bifurcations. *J. Fluid Mech.* **90**, 377–395.

JOSEPH, D. D. 1976 *Stability of Fluid Motions II*. Springer Tracts in Natural Philosophy, vol. 28, p. 138. Springer.

KELLY, R. E. & PAL, D. 1976 Thermal convection within non-uniformly heated horizontal surfaces. In *Proc. 1976 Heat Transfer and Fluid Mech. Inst.*, pp. 1–17. Stanford University Press.

KELLY, R. E. & PAL, D. 1978 Thermal convection with spatially periodic boundary conditions: resonant wavelength excitation. *J. Fluid Mech.* **86**, 433–456.

LAPWOOD, E. R. 1948 Convection of a fluid in a porous medium. *Proc. Camb. Phil. Soc.* **44**, 508–521.

LOWE, M., ALBERT, B. S. & GOLLUB, J. P. 1986 Convective flows with multiple spatial periodicities. *J. Fluid Mech.* **173**, 253–272.

LOWE, M. & GOLLUB, J. P. 1985*a* Solitons and the commensurate–incommensurate transition in a convecting nematic fluid. *Phys. Rev.* A **31**, 3893–3897.

LOWE, M. & GOLLUB, J. P. 1985*b* Pattern selection near the onset of convection: the Eckhaus instability. *Phys. Rev. Lett.* **55**, 2575–2578.

LOWE, M., GOLLUB, J. P. & LUBENSKY, T. C. 1983 Commensurate and incommensurate structures in a nonequilibrium system. *Phys. Rev. Lett.* **51**, 786–789.

NEWELL, A. C. & WHITEHEAD, J. A. 1969 Finite bandwidth, finite amplitude convection. *J. Fluid Mech.* **38**, 279–303.

PAL, D. & KELLY, R. E. 1978 Thermal convection with spatially periodic non-uniform heating: non-resonant wavelength excitation. In *Proc. 6th Intl Heat Transfer Conf., Toronto*, vol. 2.

PAL, D. & KELLY, R. E. 1979 Three dimensional thermal convection produced by two-dimensional thermal forcing. *ASME Paper* 79-HT-109.

REES, D. A. S. & RILEY, D. S. 1986 Free convection in an undulating saturated porous layer: resonant wavelength excitation. *J. Fluid Mech.* **166**, 503–530.

REES, D. A. S. & RILEY, D. S. 1989 The effects of boundary imperfections on free convection in a saturated porous layer: non-resonant wavelength excitation. *Proc. R. Soc. Lond.* A **421**, 303–339.

STRAUS, J. M. 1974 Large amplitude convection in porous media. *J. Fluid Mech.* **64**, 51–63.

TAVANTZIS, J., REISS, E. L. & MATKOWSKY, B. J. 1978 On the smooth transition to convection. *SIAM J. Appl. Maths* **34**, 322–337.

VOZOVOI, L. P. & NEPOMNYASCHII, A. A. 1974 Convection in a horizontal layer in the presence of spatial modulation of the temperature at the boundaries. *Gidrodinamika* **8**, 105–117.

WALTON, I. C. 1982 The effects of slow spatial variations on Bénard convection. *Q. J. Mech. Appl. Maths* **35**, 33–48.

WYNNE, M. C. 1987 The effects of boundary imperfections on free convection in fluid layers. Ph.D. dissertation, University of Bristol.

ZALESKI, S. 1984 Cellular patterns with boundary forcing. *J. Fluid Mech.* **149**, 101–125.